

Automatic Calibration of a Stationary Network of Laser Range Finders by Matching Movement Trajectories

Konrad Schenk, Alexander Kolarow, Markus Eisenbach, Klaus Debes, and Horst-Michael Gross*

Abstract—Laser based detection and tracking of persons can be used for numerous tasks. While a single laser range finder (LRF) is sufficient for detecting and tracking persons on a mobile robot platform, a network of multiple LRF is required to observe persons in larger spaces. Calibrating multiple LRF into a global coordinate system is usually done by hand in a time consuming procedure. An automatic calibration mechanism for such a sensor network is introduced in this paper. Without the need of prior knowledge about the environment, this mechanism is able to obtain the positions and orientations of all LRF in a global coordinate system. By comparing person tracks, determined for each individual LRF unit and matching them, constraints between the LRF units can be calculated. We are able to estimate the poses of all LRF by resolving these constraints. We evaluate and compare our method to the current state of the art approach methodically and experimentally. Experiments show that our calibration approach outperforms this approach.

I. INTRODUCTION

Detecting and tracking moving objects with laser range finders (LRF) yield a lot of applications in the field of mobile robotics. They are usually installed on robotic platforms to provide the robot with information about its surroundings. But also static installations of LRF became common in the last years [1], [2], [3]. In mobile robotics, they can be used to obtain ground truth data for the robot, or help in navigation [4]. Also applications for benchmarking the navigation behavior of a robot are possible, as for example evaluating self localization algorithms and tracking mechanisms, as we did during the "EU Robotics Week" [5]. A set of four stationary LRF was used for precisely tracking a robot in a domestic environment for several days, evaluating its self localization and navigation behavior. Also the people around the robot were tracked in order to provide a ground truth for benchmarking the robot's visual person tracking algorithms.

By incorporating only one static LRF, the area for tracking is limited to its maximum detection range. Additionally, the tracking may be disturbed by occlusions. A simple solution to avoid occlusions and extend the range is to add more LRF to the scene. However, the positions and orientations of all laser range finders need to be known in order to continuously track persons over larger distances. Usually these poses are measured by hand. Since this procedure is very time consuming, we present a calibration algorithm,

which is able to automatically determine the positions and orientations of all laser range finders in a global coordinate system without any prior knowledge about the environment.

The remainder of this paper is organized as following: We present the state of the art for matching static and dynamic objects for calibration in Sect. II, followed by the description of the calibration algorithm in Sect. III. Additionally, we benchmark our approach and compare it to the state of the art in various challenging setups in Sect. IV. Finally, we are summarizing the results in Sect. V and giving an outlook.

II. STATE OF THE ART

In mobile robotics, localization in an unknown environment is a common problem. SLAM or other robot localization techniques [6], [7] can be used to solve it. But these techniques are only applicable for robots, since the relative positions between multiple observations are known from odometry information. When using a network of stationary sensors, the relative distances between different sensors are unknown, so robot localization methods are not applicable for the scenario of stationary sensors.

A. Using static objects for Matching

Static objects, which can be observed by multiple laser range finders, can be used as reference objects for calibration. Scan matching methods, like Polar Scan Matching (PSM) [8], Iterative Closest Point (ICP) [9], point registration methods from computer vision [10], or others [11], [12], [13], can be used to rectify the sensors. As stated in [14] the use of scan matching techniques should be avoided in our scenario, since several problems exist:

- no static object may exist, which is mutually observed by multiple LRF
- occlusions, caused by obstacles or disadvantageous arrangements
- ambiguities and symmetries in the environment may lead to false matches

Markers (e.g. reflectors for laser range finders) added to the sensors may be used as landmarks for calibrating multiple LRF, but irresolvable ambiguities or obstacles may disturb the alignment. In general, matching with static objects is not preferable as calibration method as long as no initial hypothesis is available.

B. Using dynamic objects for Matching

Dynamic objects, as for example persons walking through the scene, can be used for calibration as well. Based on tracking all persons individually for each LRF, a calibration

*This work has received funding from the German Federal Ministry of Education and Research as part of the APFEL project under grant agreement no. 13N10797.

K. Schenk, A. Kolarow, M. Eisenbach, K. Debes, and H.-M. Gross are with Neuroinformatics and Cognitive Robotics Lab, Ilmenau University of Technology, 98694 Ilmenau, Germany
konrad.schenk@tu-ilmenau.de

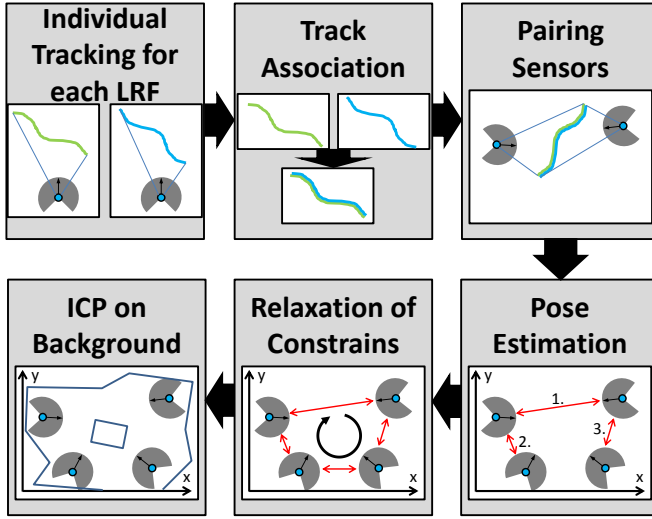


Fig. 1. General workflow of the proposed calibration method. First, all persons are tracked for each single LRF. Afterwards, tracks between the LRF are associated. After pairing all sensors with constrains, their poses are initially estimated. In order to take every constrain into account, a relaxation algorithm is applied. If a static background is available, it is used to align the LRF with ICP in a final step.

algorithm was presented in [14] and [15]. The algorithm in [14] uses several randomly picked pairs of observations of the same person to estimate the constraints between the laser range finders. In contrast to comparing a few single observations, point registration methods can be used to align the tracks. This yields into better precision for the constraints, since not only two single matches of person detections are used for triangulation, but the whole track. For matching tracks, the following methods are applicable: Longest Common Subsequence (LCS) [16], Quaternion-based Rotationally Invariant LCS (QRLCS) [17], Levenshtein Distance on trajectories [18], or track matching based on ICP [9]. The latter is used in our approach. Also a representation of tracks as feature vectors and comparing the features [19] is possible.

The calibration algorithm presented here was developed in parallel and independently to the methods of Glas et al. [14] and Sasaki et al. [15]. The algorithm of [15] cannot be compared to our approach due to insufficient evaluation in its experimental section. Also several details are not clear and, therefore, a reimplement was not possible. The general workflow of our method is similar to [14], but the implementation differs. The major differences between both approaches are

- a multiple particle filter based tracking is used in our approach instead of distance based tracking
- we applied Euclidean matching of trajectories instead of velocity based matching as presented in Glas et al. [14]
- singular value decomposition for constraint generation is used in our approach instead of triangulation
- ICP is used in our approach for final alignment

The details are addressed subsequently in the respective subsections.

III. CONSTRAINT GENERATION AND RESOLVING

In order to calibrate the sensor network, six tasks are performed (see Fig. 1). At first, the tracks of people need to be recorded for each laser range finder (Sect. III-A). By comparing these tracks, mutual observations between the LRF units are detected (Sect. III-B). Based on the mutual observations, constraints between LRF units are identified (Sect. III-C). The main calibration step is performed by resolving these constraints (Sect. III-D). An additional relaxation algorithm is included to resolve multiple constraints (Sect. III-E). In order to improve the calibration, a final ICP-alignment is performed, if a static background is available (Sect. III-F).

A. Tracking

In order to obtain tracks for each person, tracking needs to be performed for each LRF in its local cartesian coordinate system. Almost any tracking method, which extracts the individual tracks of persons from laser range data in real-time [2], [20], [21], is suitable for our calibration method. The tracking algorithm we have chosen applies a histogram based background subtraction on the range data in order to get detections of people [21]. Multiple particle filters are applied to track persons independently, as described in [21].

After tracking people for an initial period, their tracks can be used to identify mutual observations between laser range finders.

B. Track Association

For each pair (m, n) of LRF, their tracks are compared in order to find pairs, belonging to the same person. In Glas et al. [14], the tracks are compared by their velocity profile. Since matching tracks by velocity holds more occasions for false associations as matching them by mean Euclidean distance after alignment, we followed the latter approach. Not only the geometrical shapes are considered this way, but also the velocities are incorporated indirectly by the distance between two adjacent sampling points.

A track $T_a = (\mathbf{p}_{1,a}, \mathbf{p}_{2,a}, \dots, \mathbf{p}_{N,a})$ consists of N sampling points $\mathbf{p}_{i,a} = (x_{i,a}, y_{i,a}, t_i)^T, i = 1, \dots, N$, where $(x_{i,a}, y_{i,a})^T$ is the position of the person a at the time t_i . Before associating the tracks of two LRF, all tracks from LRF m are paired with all tracks from LRF n . Afterwards, the two tracks T_a^m and T_b^n of each pair are trimmed to the period, where they have an overlap in time. Since our sensor network is synchronized in time, the two resulting tracks \tilde{T}_a^m and \tilde{T}_b^n are sampled at the same time steps and have the same amount of sampling points. Now, they can be easily aligned onto each other and the mean Euclidean distance between their sampling points is calculated.

A track \tilde{T}_a^m can be aligned onto another track \tilde{T}_b^n by transforming its sampling points $\mathbf{p}_{i,a}$ to $\hat{\mathbf{p}}_{i,a}$ according to Eq. 1, with $\phi_{a,b}$ being the optimal rotation and $(x_{a,b}, y_{a,b})^T$ the optimal translation.

$$\hat{\mathbf{p}}_{i,a} = \begin{pmatrix} \cos(\phi_{a,b}) & \sin(\phi_{a,b}) & 0 \\ -\sin(\phi_{a,b}) & \cos(\phi_{a,b}) & 0 \\ 0 & 0 & 1 \end{pmatrix} \cdot \left(\mathbf{p}_{i,a} - \begin{pmatrix} x_{a,b} \\ y_{a,b} \\ 0 \end{pmatrix} \right) \quad (1)$$

The optimal rotation and translation can be calculated by minimizing the mean Euclidean distance $d_{a,b}$ (see Eq. 2) with an approach introduced in [9] and [22]. It uses singular value decomposition for registering two point sets.

$$d_{a,b} = \frac{\sum_{i=1}^N \sqrt{(\hat{x}_{i,a} - x_{i,b})^2 + (\hat{y}_{i,a} - y_{i,b})^2}}{N} \quad (2)$$

After aligning two tracks \tilde{T}_a^m and \tilde{T}_b^n , they are considered belonging to the same person, if their distance $d_{a,b}$ is below an experimentally evaluated threshold of 20 cm.

C. Pairing Sensors

Based on all pairs of tracks belonging to the same person, relative positions between sensor nodes can be calculated for each pair of LRF independently. Glas et al. [14] uses only the positions of people for the current iteration and a randomly picked previous observation to constrain pairs of LRF units. With a pair of observations, the relative positions of both laser range finders can be triangulated (see Fig. 2 on the left side). In contrast to this approach, we incorporated whole tracks for alignment (see Fig. 2 on the right side). At first, all matched Tracks \tilde{T}_j^m and \tilde{T}_j^n , $j = 1, \dots, J$ of LRF unit m and n are joined into two virtual tracks T_m and T_n with Eq. 3.

$$T_m = (\tilde{T}_1^m, \tilde{T}_2^m, \dots, \tilde{T}_J^m) \quad (3)$$

Since the matched Tracks are synchronized in time and are of the same length, the resulting virtual tracks are also synchronized in time and of the same length. Therefore, they can easily be aligned onto each other using the same procedure, described in III-B. The resulting optimal rotation $\check{\phi}_{m,n}$, translation $(\check{x}_{m,n}, \check{y}_{m,n})^T$ and their distance $d_{m,n}$ can be used to form a constraint for the corresponding pair of laser range finders. A constraint for LRF units m and n contains the relative pose $\check{\theta}_{m,n} = (\check{x}_{m,n}, \check{y}_{m,n}, \check{\phi}_{m,n})^T$ of unit m in the local space of unit n and $\theta_{n,m}$ vice versa. Additionally, a weight $w_{m,n}$ is calculated for the constraint according to Eq. 4, with N being the amount of sampling points of T_m . Long matched tracks with a small distance in matching results in a higher weight than short matched tracks with a big distance in matching. Therefore, the weight of a constraint depicts its confidence.

$$w_{m,n} = \frac{N}{d_{m,n}} \quad (4)$$

D. Pose Estimation

All LRF pairs are sorted in descending order of their weight $w_{m,n}$. One LRF unit of the pair with the highest weight is placed at the origin of the global coordinate system. The other unit is then placed correspondingly to their constraint. Afterwards, every other pair containing one LRF unit, which is already placed, is aligned iteratively. If $\theta_m = (x_m, y_m, \phi_m)^T$ is the pose of a placed LRF unit, $\theta_n = (x_n, y_n, \phi_n)^T$ can be computed with Eq. 5. This is

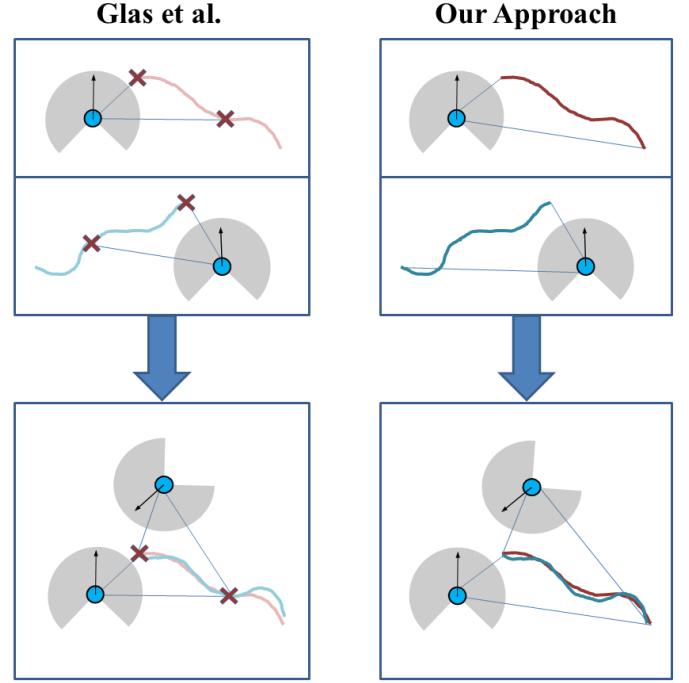


Fig. 2. Aligning a pair of LRF units. On the left side, two mutual observations (marked as crosses) were taken for alignment as described in Glas et al. [14]. The alignment minimizes the distance between both observations.

On the right side, two tracks are associated, and the LRF units are aligned accordingly, as described in this paper. The alignment minimizes the distance between all sampling points of the two tracks.

done, until all LRF are placed.

$$\theta_n = \begin{pmatrix} \cos(-\phi_m) & \sin(-\phi_m) & 0 \\ -\sin(-\phi_m) & \cos(-\phi_m) & 0 \\ 0 & 0 & 1 \end{pmatrix} \cdot \check{\theta}_{n,m} + \theta_m \quad (5)$$

E. Relaxation

Additionally, the relaxation algorithm introduced in [23] refines all constraints iteratively, after the initial pose estimation. This procedure takes every constraint into account and, therefore, closes loops in constraints. This approach was adopted for our algorithm in order to improve the results. For each LRF m , new positions $(x_{m,n}, y_{m,n})$ are estimated with Eq. 6 based on all neighboring LRF $n = 1, \dots, L$ and the corresponding constraints $\check{\theta}_{m,n}$.

$$\begin{aligned} x_{m,n} &= x_n + \cos(-\phi_n) \cdot \check{x}_{m,n} + \sin(-\phi_n) \cdot \check{y}_{m,n} \\ y_{m,n} &= y_n - \sin(-\phi_n) \cdot \check{x}_{m,n} + \cos(-\phi_n) \cdot \check{y}_{m,n} \end{aligned} \quad (6)$$

Afterwards, a weight $v_{m,n}$ is calculated for each position estimate, based on the weight of each neighbor w_n and the weight $w_{m,n}$ of the corresponding constraint according to Eq. 7.

$$v_{m,n} = \frac{w_n \cdot w_{m,n}}{w_n + w_{m,n}} \quad (7)$$

After calculating all position estimates and their weights for all LRF, a new weight w_m and position (x_m, y_m) for a LRF m can be calculated with Eq. 8 and Eq. 9.

$$w_m = \sum_{n=1}^L v_{m,n} \quad (8)$$

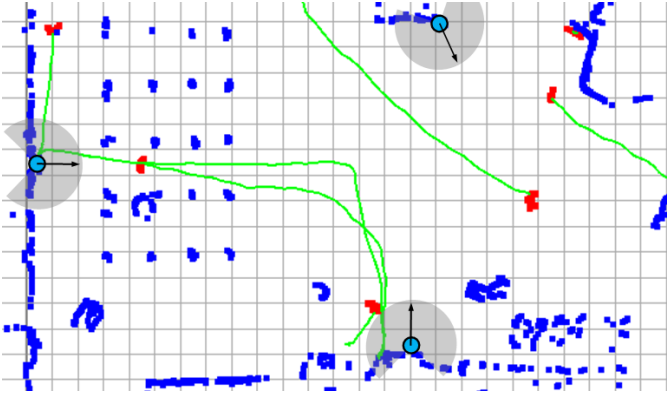


Fig. 3. Calibrated scene utilizing three laser range finders at the Erfurt-Weimar airport, Germany. Calibration was done during daily operation. The background scans are colored blue and the foreground scans are colored red. The LRF and their coverage angles are shown as gray arcs. The tracks of all persons are shown green.

$$x_m = \sum_{n=1}^L \frac{x_{m,n} \cdot v_{m,n}}{w_m} \quad y_m = \sum_{n=1}^L \frac{y_{m,n} \cdot v_{m,n}}{w_m} \quad (9)$$

Finally, the rotations ϕ_m are adjusted by minimizing Eq. 10.

$$\phi_m = \underset{\phi}{\operatorname{argmin}} \left(\sum_{n=1}^L \left| \left(\phi + \check{\phi}_{n,m} \right) - \operatorname{atan} \left(\frac{y_n - y_m}{x_n - x_m} \right) \right| \right) \quad (10)$$

F. Final ICP Alignment

For a laser range finder, a person is only observable from one side. Therefore, the tracking mechanism may have an offset, depending of the angle from which the person is observed. This also results in an offset of the calibration. To counteract the offset and further improve the calibration accuracy, an ICP algorithm is applied on the scan points of each laser range finder. Only points classified as background by the background subtraction, mentioned in III-A, are used

for alignment. The generic ICP assigns a point from the target set to every point from the source set and performs a transformation in order to minimize the distances between them iteratively [9]. Since the overlap between laser range finders is usually small, such a procedure would seriously thwart the calibration. In contrast to the basic ICP, as presented in [9], we only take points into account, which are close to each other. This way, only scan points which may be caused by the same observed object are tightened.

IV. EXPERIMENTS

We already employed the calibration in several situations utilizing multiple LRF for benchmarking reidentification [24], for vision-based tracking [25] and shown in Fig. 3. Since no precise ground truth for the LRF poses was obtainable in these situations, we conducted several experiments at our lab to evaluate the calibration performance. We recorded 13 sequences at two locations with four setups. The first location represents an open space, at which calibration yields no difficulties. The second location is used to test the calibration under more challenging situations in corridors with junctions. In the first location, we used two setups. Setup *A* (see Fig. 4(a)) covers an area of approximately $15\text{m} \times 6\text{m}$ where a person can be observed by every LRF at almost any time. Setup *B* (see Fig. 4(b)) was designed to force errors in alignment to sum up. It covers an area of approximately $30\text{m} \times 6\text{m}$ with the LRF placed in a chain. In the second location, we also used two setups. In setup *C* (see Fig. 4(c)), we placed the LRF with an overlap as large as possible while covering the whole area. It is assumed, that closing loops in constraints with relaxation help improving the calibration results. Setup *D* (see Fig. 4(d)) was chosen to give a more challenging situation since the overlap between the most right LRF is diminished.

A. Conducted Experiments

An overview of the conducted experiments is shown in Table I. Additionally, the walking paths in setup *C* and *D*

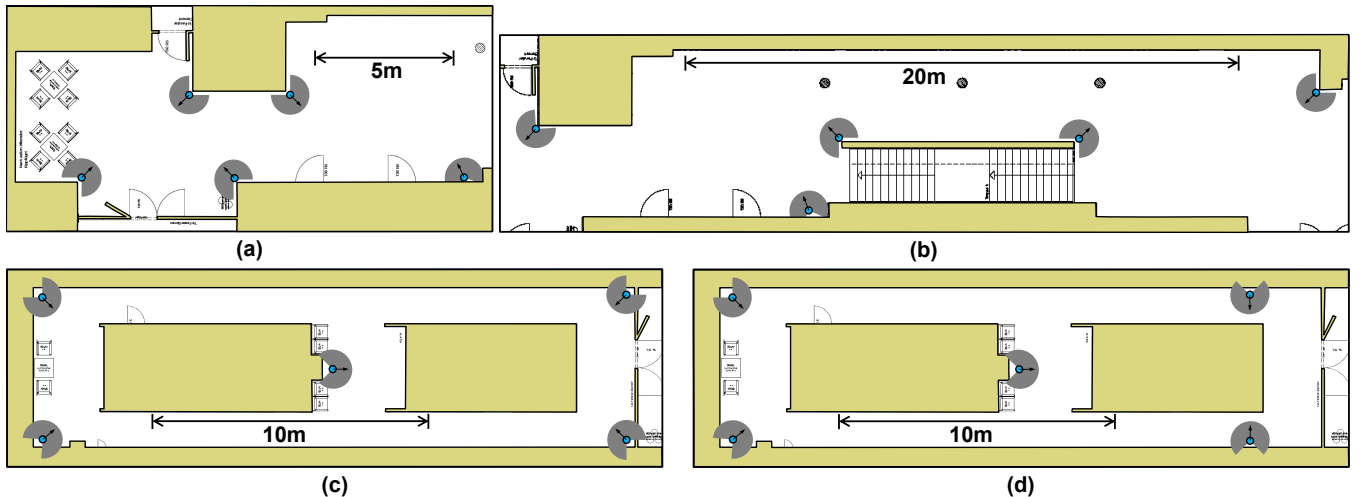


Fig. 4. Overview of the four LRF setups used in our experiments. The LRF and their coverage angles are shown as gray arcs.

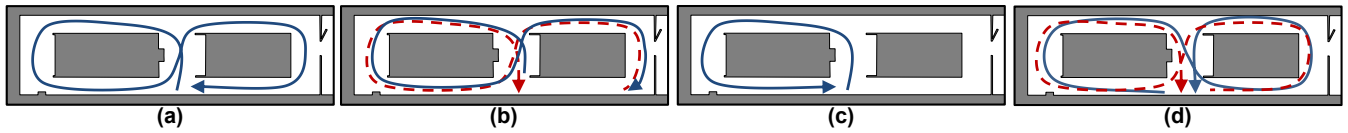


Fig. 5. Walking paths in setup *C* and *D* (see Fig. 4). In (a), a single person (shown blue) walked an eight-shaped path through the corridors. In (b), two persons (shown red and blue) walked an eight-shaped path in opposite directions. In (c), a single person (shown blue) walked around the left block. In (d), two persons (shown red and blue) walked an eight-shaped path in mirrored directions.

are depicted in Fig. 5.

For the addressed setups, we used five laser range finders LMS151 from SICK. They scan 270° with a 0.5° resolution at 50 Hz and a maximum range of 50 m. The ground truth was obtained by manually measuring their positions. The LMS151 has an internal clock and tags every scan data with a timestamp, enabling us to compensate for delays, caused by the network, with time synchronization. In order to synchronize the clocks of the LRF and the receiving computer, the offset between the two clocks needs to be known. Local Area Networks usually have round-trip-times lower than the time between two laser scans, which is 20 ms. Therefore, it is sufficient to maintain the minimum offset observed between the timestamp of a laser scan and the time of reception at the computer. The residual error may be addressed with more sophisticated methods, but this simple solution proved to be sufficient in our scenario.

B. Results and Discussion

For evaluation, each scenario was calibrated 1,000 times, and the final result of every calibration belonging to one scenario was examined. The translational and rotational errors were calculated. The mean and standard deviation of all 1,000 translational and rotational errors for each scene are shown in Table II. Exemplary, the calibration error over time of a reimplementation of [14] and our approach is shown for scene *B2* in Fig. 6.

In order to provide a fair comparison, we used the same synchronized data for evaluating our approach and the algo-

rithm presented in [14].

First of all, it can be seen that our approach performs excellent in easy settings (Scene *A* and *B* in Table II). Even in scene *B*, where the LRF are placed in a chain and errors may sum up, the alignment is as good as in the easier scene *A*. Since the calibration errors are within the measurement errors of the used type of laser range finders (systematic error of $\pm 3\text{cm}$ and a statistical error of $\pm 1.2\text{cm}$), the calibration of our approach can be considered perfect in scenes *A* and *B*. Additionally, the rotational error is below the angular resolution of the used LRF. The method of Glas et al. [14] performs only slightly worse compared to our approach.

The algorithm presented in [14] performed poorly in scene *C* and *D*. In some cases the algorithm was not able to align all five LRF (marked with a “—”). The missing LRF was always the one standing in the middle corridor (Fig. 4(c,d)). Its overlapping areas to the other four LRF are very small, and mutual observations only appear for a short time. Since the algorithm in [14] does not take observations continuously, there is only a small chance to sample more than one mutual observation with another LRF. Also matching tracks based on the velocities leads to more confusions as matching them by shape, as the results in *C2*, *D2* and *D3* show.

Our approach was able to obtain good calibration results in difficult scenes (*C* and *D*). The standard deviation of the alignment error shows that a few calibrations failed (*C2*). The tracks of both persons are similar in scene *C2* (see Fig. 5(b): turning left followed by turning right). Thus, two distant LRF with no overlapping scan areas are sometimes

Pattern	Setup (Fig. 4)			
	A	B	C	D
walking straight from left to right and back with constant speed	A1	B1		
tottering around to cover a large area	A2	B2		
walking with varying speed from left to right and back	A3			
randomly strolling around for a minute	A4			
one person walking an eight (see Fig. 5(a))			C1	D1
two persons walking an eight in opposite directions (see Fig. 5(b))			C2	D2
one person walking around the left block (see Fig. 5(c))			C3	
two persons walking an eight in mirrored directions (see Fig. 5(d))			C4	D3

TABLE I

OVERVIEW OVER DIFFERENT SETUPS USED IN OUR EXPERIMENTS. THE USED LOCATION AND LRF PLACEMENT (A TO D) CAN BE SEEN IN FIG. 4

Setup	our approach				Glas et al. [14]			
	positional error in cm mean	std	rotational error in $^\circ$ mean	std	positional error in cm mean	std	rotational error in $^\circ$ mean	std
A1	2.1	0.3	0.3	<0.1	33.5	3.9	1.0	0.5
A2	2.0	0.3	0.2	0.1	8.8	2.2	0.5	0.2
A3	1.9	0.3	0.3	<0.1	8.1	2.0	0.5	0.3
A4	1.6	0.3	0.3	0.1	6.5	2.1	0.5	0.3
B1	1.9	0.5	0.2	<0.1	7.5	2.6	0.5	0.2
B2	1.5	0.5	0.2	<0.1	10.3	3.3	0.6	0.3
C1	9.2	4.7	0.7	0.6	—	—	—	—
C2	86.5	154	5.8	10.6	583	257	58.2	19.7
C3	34.8	8.2	4.4	1.5	—	—	—	—
C4	66.6	42.9	6.8	7.3	—	—	—	—
D1	47.9	26.8	3.4	2.2	—	—	—	—
D2	90.4	58.1	4.0	4.5	488	36.1	54.6	8.0
D3	29.3	20.3	3.7	7.5	561	177	38.6	15.6

TABLE II

CALIBRATION ERRORS OF OUR APPROACH COMPARED TO THE ALGORITHM PRESENTED IN GLAS ET AL. [14]

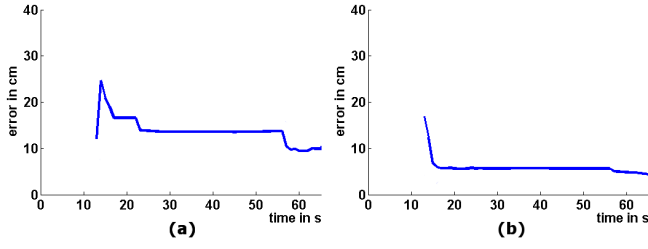


Fig. 6. Calibration error of scene *B2* over time. In (a), the error of the method by Glas et al. [14] is shown. In (b), the error of our approach is presented. After $t = 13$ s, all LRF have observed mutual tracks and the first alignment was done.

matching their tracks by mistake due to their almost similar shape. These false matches are causing erroneous constraints leading to large errors in calibration. This problem may be addressed by observing the scene for a longer time. As long, as ambiguous tracks are outnumbered by unique tracks, our approach is able to calibrate correctly. A more sophisticated algorithm for registration of two point sets, as for example [26], can also be used to compensate for false matches. In *C4* and *D3*, the tracks of both persons are mirrored (see Fig. 5(d)). Therefore, their shapes are different, even if the velocity profile, which is used for matching in [14], is similar. Since our approach applies a track assignment incorporating the shapes, false assignments are prevented and the obtained constraints are acceptable.

We additionally calculated the positional errors before the ICP step was applied to evaluate its influence on the quality of calibration. The comparison of our approach with ICP to our approach without ICP is shown in Table III. It can be seen that ICP improves the calibration, if a good initial estimation was found (Setup *A* and *B*). If the estimation is

Setup	our approach with ICP				our approach without ICP			
	positional error in cm		rotational error in °		positional error in cm		rotational error in °	
	mean	std	mean	std	mean	std	mean	std
A1	2.1	0.3	0.3	<0.1	5.4	0.7	0.2	0.2
A2	2.0	0.3	0.2	0.1	5.6	0.6	0.5	0.3
A3	1.9	0.3	0.3	<0.1	4.5	0.9	0.2	0.2
A4	1.6	0.3	0.3	0.1	4.1	0.9	0.4	0.2
B1	1.9	0.5	0.2	<0.1	4.8	1.2	0.4	0.2
B2	1.5	0.5	0.2	<0.1	4.5	1.0	0.4	0.2
C1	9.2	4.7	0.7	0.6	10.2	5.0	1.2	0.9
C2	86.5	154	5.8	10.6	83.2	156	5.6	10.6
C3	34.8	8.2	4.4	1.5	22.0	5.8	4.0	1.3
C4	66.6	42.9	6.8	7.3	70.6	44.5	6.8	7.4
D1	47.9	26.8	3.4	2.2	45.5	26.9	2.9	2.2
D2	90.4	58.1	4.0	4.5	80.4	63.6	3.3	4.5
D3	29.3	20.3	3.7	7.5	29.4	20.7	3.4	7.3

TABLE III

INFLUENCE OF ICP ON THE CALIBRATION ERROR. IT CAN BE SEEN THAT ICP IMPROVES THE CALIBRATION, IF A GOOD INITIAL ESTIMATION WAS FOUND.

only moderate (Setup *C* and *D*), ICP is not always able to improve the results. Some examples of ICP alignment are depicted in Fig. 7 and 8.

Finally, our calibration algorithm shows perfect results in ordinary situations with a lot of scan overlap (Setup *A* and *B*). In challenging situations (Setup *C* and *D*), the limits of our approach are perceivable but calibration still succeeded. Even if no controlled conditions are possible, as shown in Fig. 3, calibration succeeds. The advantages of shape-based track matching and full track alignment, as used in our calibration method, could be successfully demonstrated.

V. CONCLUSION AND OUTLOOK

We have proposed a new method for calibrating multiple LRF units into a global coordinate system by observing person tracks without any knowledge about the environment. Furthermore, we evaluated the performance on 13 different scenes and compared it to the state of the art algorithm, presented in Glas et al. [14]. Our experiments show, that our method outperforms [14] in easy settings as well as in difficult scenes. The results in ordinary scenes can be considered to be perfect. We also conclude, that post processing the results with ICP improves the alignment.

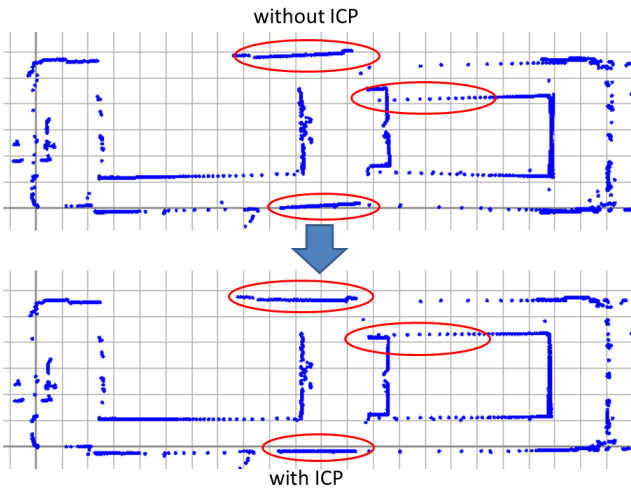


Fig. 7. Scan points of setup *C* in top view. The grid has a resolution of 1 m. In the upper part, our calibration was stopped after relaxation. In the lower part, an additional ICP alignment was performed. The ICP alignment was able to rectify the positional offset as it can be seen in the marked areas.

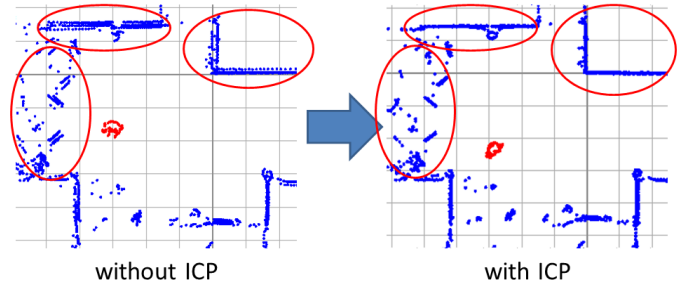


Fig. 8. Scan points of setup *A* in top view. The grid has a resolution of 1 m. On the left side, our calibration was stopped after relaxation. On the right side, an additional ICP alignment was performed. It can be seen (red marks), that small positional offsets of the LRF units can be eliminated.

REFERENCES

- [1] T. Kanda, D. F. Glas, M. Shiomi, H. Ishiguro, and N. Hagita, "Who will be the customer?: A social robot that anticipates people's behavior from their trajectories," in *UbiComp*, pp. 380–389, 2008.
- [2] X. Shao, K. Katabira, R. Shibasaki, H. Zhao, and Y. Nakagawa, "Tracking a variable number of pedestrians in crowded scenes by using laser range scanners," in *IEEE International Conference on Systems, Man, and Cybernetics*, pp. 1545–1551, 2008.
- [3] X. Song, X. Shao, R. Shibasaki, H. Zhao, J. Cui, and H. Zha, "A novel laser-based system: Fully online detection of abnormal activity via an unsupervised method," in *Robotics and Automation (ICRA), 2011 IEEE International Conference on*, pp. 1317–1322, may 2011.
- [4] D. F. Glas, T. Kanda, H. Ishiguro, and N. Hagita, "Simultaneous people tracking and localization for social robots using external laser range finders," in *IEEE/RSJ International Conference on Intelligent Robots and Systems*, pp. 846–853, 2009.
- [5] EU Robotics Week. <http://www.eurobotics-project.eu/eurobotics-week/index.html>, 2011.
- [6] H.-M. Gross, A. Koenig, and S. Mueller, "Omniview-based concurrent map building and localization using adaptive appearance maps," in *IEEE International Conference on Systems, Man, and Cybernetics*, pp. 3510–3515, 2005.
- [7] J. Porta and B. Kroese, "Appearance-based concurrent map building and localization using a multi-hypotheses tracker," in *IEEE/RSJ International Conference on Intelligent Robots and Systems*, pp. 3424–3429, 2004.
- [8] A. Diosi and L. Kleeman, "Laser scan matching in polar coordinates with application to slam," in *IEEE/RSJ International Conference on Intelligent Robots and Systems*, pp. 3317–3322, 2005.
- [9] P. Besl and D. McKay, "A method for registration of 3-d shapes," *IEEE Transactions on Pattern Analysis and Machine Intelligence*, vol. 14, pp. 239–256, 1992.
- [10] B. Jian and B. Vemuri, "Robust point set registration using gaussian mixture models," *IEEE Transactions on Pattern Analysis and Machine Intelligence*, pp. 1633–1645, 2011.
- [11] N. Ripperda and C. Brenner, "Marker-free registration of terrestrial laser scans using the normal distribution transform," in *ISPRS Working Group V/4 Workshop 3D-ARCH*, 2005.
- [12] T. Rofer, "Using histogram correlation to create consistent laser scan maps," in *IEEE/RSJ International Conference on Intelligent Robots and Systems*, pp. 625–630, 2002.
- [13] G. Weiss and E. Puttkamer, "A map based on laser scans without geometric interpretation," in *Intelligent Autonomous Systems 4*, pp. 403–407, 1995.
- [14] D. Glas, T. Miyashita, H. Ishiguro, and N. Hagita, "Automatic position calibration and sensor displacement detection for networks of laser range finders for human tracking," in *IEEE/RSJ International Conference on Intelligent Robots and Systems*, pp. 2938–2945, 2010.
- [15] T. Sasaki and H. Hashimoto, "Calibration of laser range finders based on moving object tracking in intelligent space," in *Networking, Sensing and Control, 2009. ICNSC '09. International Conference on*, pp. 620–625, march 2009.
- [16] M. Vlachos, G. Kollios, and D. Gunopulos, "Elastic translation invariant matching of trajectories," *Machine Learning*, pp. 301–334, 2005.
- [17] C. Hermes, C. Woehler, K. Schenk, and F. Kummert, "Long-term vehicle motion prediction," in *IEEE Intelligent Vehicles Symposium*, pp. 652–657, 2009.
- [18] M. Hahn, L. Krueger, and C. Woehler, "3d action recognition and long-term prediction of human motion," in *Computer Vision Systems*, vol. 5008, pp. 23–32, 2008.
- [19] X. Li, W. Hu, and W. Hu, "A coarse-to-fine strategy for vehicle motion trajectory clustering," in *International Conference on Pattern Recognition*, pp. 591–594, 2006.
- [20] J. Lee, T. Tsubouchi, K. Yamamoto, and S. Egawa, "People tracking using a robot in motion with laser range finder," in *IEEE/RSJ International Conference on Intelligent Robots and Systems*, pp. 2936–2942, 2006.
- [21] K. Schenk, M. Eisenbach, A. Kolarow, and H.-M. Gross, "Comparison of laser-based person tracking at feet and upper-body height," in *34th Annual Conference on Artificial Intelligence (KI)*, vol. 7006, pp. 277–288, 2011.
- [22] J. Martinez, J. Gonzalez, J. Morales, A. Mandow, and A. Garcia-Cerezo, "Mobile robot motion estimation by 2d scan matching with genetic and iterative closest point algorithms," *Journal of Field Robotics*, pp. 21–34, 2006.
- [23] T. Duckett, S. Marsland, and J. Shapiro, "Learning globally consistent maps by relaxation," in *IEEE International Conference on Robotics and Automation*, pp. 3841–3846, 2000.
- [24] M. Eisenbach, A. Kolarow, K. Schenk, K. Debes, and H. Gross, "View invariant appearance-based person reidentification using fast online feature selection and score level fusion," in *9th IEEE International Conference on Advanced Video and Signal-Based Surveillance (AVSS)*, 2012.
- [25] A. Kolarow, M. Brauckmann, M. Eisenbach, K. Schenk, E. Einhorn, K. Debes, and H. Gross, "Vision-based hyper-real-time object tracker for robotic applications," in *IEEE/RSJ International Conference on Intelligent Robots and Systems*, 2012.
- [26] H. Li, T. Shen, and X. Huang, "Approximately global optimization for robust alignment of generalized shapes," *Pattern Analysis and Machine Intelligence, IEEE Transactions on*, vol. 33, no. 6, pp. 1116–1131, 2011.